Electronic Supplementary Material (ESI) for Journal of Materials Chemistry C.
This journal is © The Royal Society of Chemistry 2019

Iridium(III) phosphors with rigid fused-heterocyclic chelating architecture for efficient deep-red/near-infrared emission in polymer light-emitting diodes

Caifa You,[a] Denghui Liu,[b] Fanyuan Meng,[c] Yafei Wang,[b] Junting Yu,[b] Song Wang,*[d] Shijian Su*[c] and Weiguo Zhu*[a,b]

[a] *College of Chemistry, Key Lab of Environment-Friendly Chemistry and Application in the Ministry of Education, Xiangtan University, Xiangtan 411105, China.*

[b] *School of Materials Science and Engineering, Jiangsu Collaboration Innovation Center of Photovoltaic Science and Engineering, Jiangsu Engineering Laboratory of Light-Electricity-Heat Energy-Converting Materials and Applications, National Experimental Demonstration Center for Materials Science and Engineering, Changzhou University, Changzhou 213164, P. R. China.*

[c] *State Key Laboratory of Luminescent Materials and Devices, South China University of Technology, Guangzhou 510640, P. R. China.*

[d] *Hubei Key Laboratory of Low Dimensional Optoelectronic Materials and Devices Hubei University of Arts and Science, Xiangyang, 441053, P. R. China.*

**To whom correspondence should be addressed. Email:*

(W. Z.) zhuwg18@126.com

(S. S.) mssjsu@scut.edu.cn

(S. W.) wangsong1984@126.com

Contents of Figures and Tables

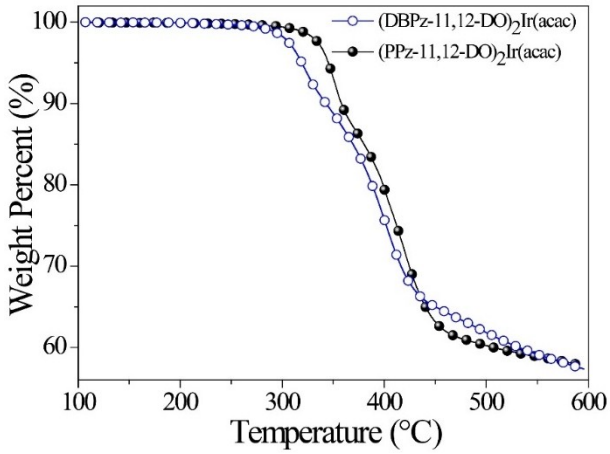

Fig. S1. TGA curves of Ir(III) complexes under nitrogen atmosphere.

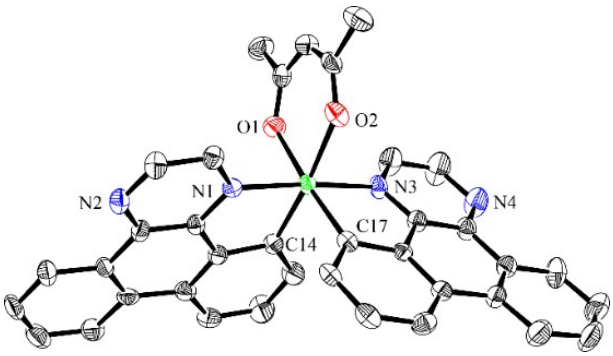

Fig. S2. ORTEP plot of $(DBQ)_2Ir(acac)$ with 50% probability ellipsoids, Hydrogen atoms are omitted for clarity.

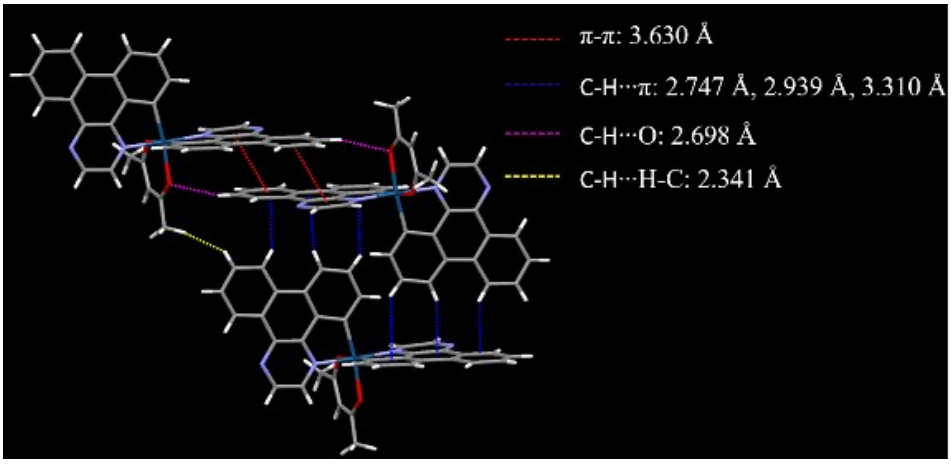

Fig. S3. The crystal-packing diagram of $(DBQ)_2Ir(acac)$ (π-π, C-H···π, C-H···O and C-H···H···C intermolecular interactions are marked by dashed lines).

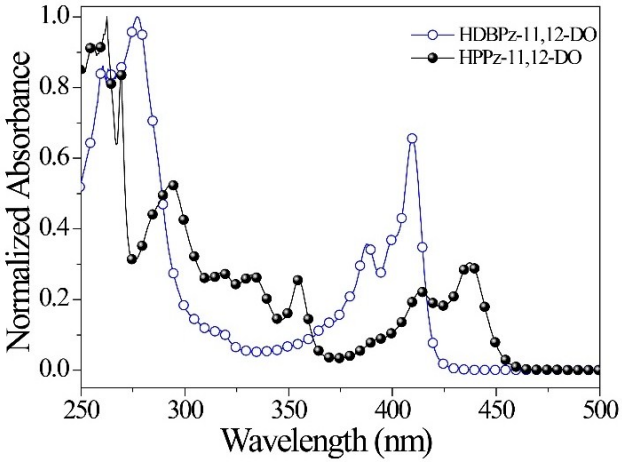

Fig. S4. UV-Vis absorption spectra of free ligands in DCM at RT.

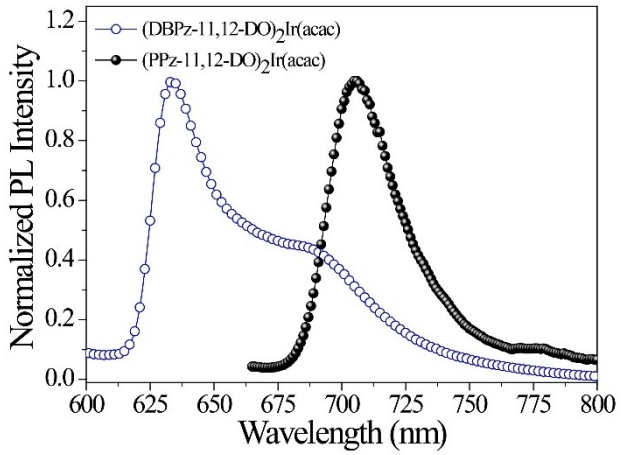

Fig. S5. Normalized emission spectra of Ir(III) complexes in dilute 2-MeTHF (10^{-5} M) at 77 K.

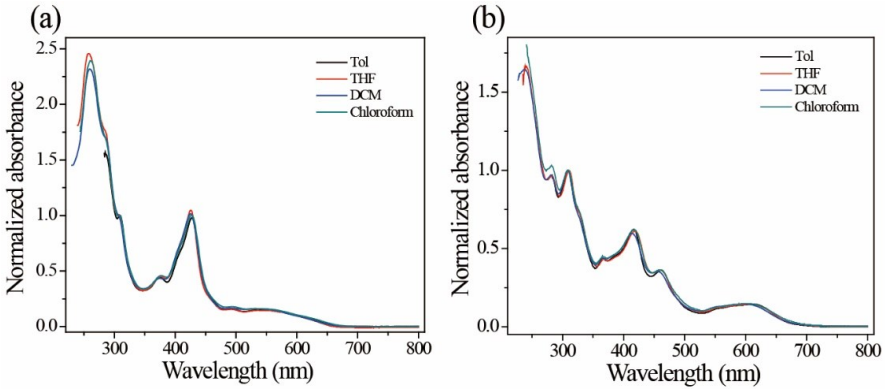

Fig. S6. Normalized absorption spectra of Ir(III) complexes in various solvents at RT, $(DBPz\text{-}11,12\text{-}DO)_2Ir(acac)$ (a) and $(PPz\text{-}11,12\text{-}DO)_2Ir(acac)$ (b).

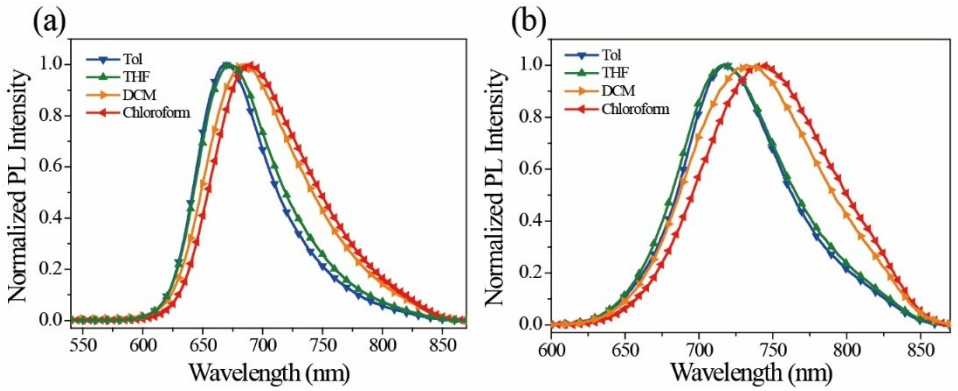

Fig. S7. Normalized emission spectra of the two Ir(III) complexes in various degassed solvents at RT, (a) $(DBPz\text{-}11,12\text{-}DO)_2Ir(acac)$, Ex=420 nm; and (b) $(PPz\text{-}11,12\text{-}DO)_2Ir(acac)$, Ex=450 nm.

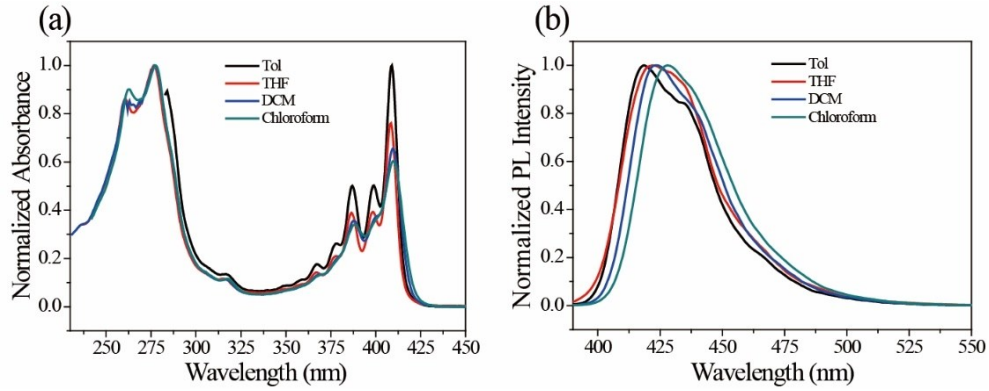

Fig. S8. Normalized absorption (a) and emission (b) spectra of HDBPz-11,12-DO in various solvents, Ex=380 nm.

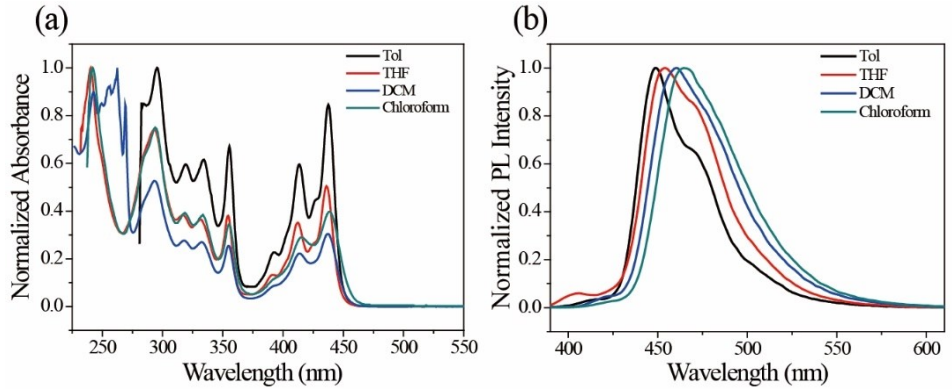

Fig. S9. Normalized absorption (a) and emission (b) spectra of HPPz-11,12-DO in various solvents, Ex=350 nm.

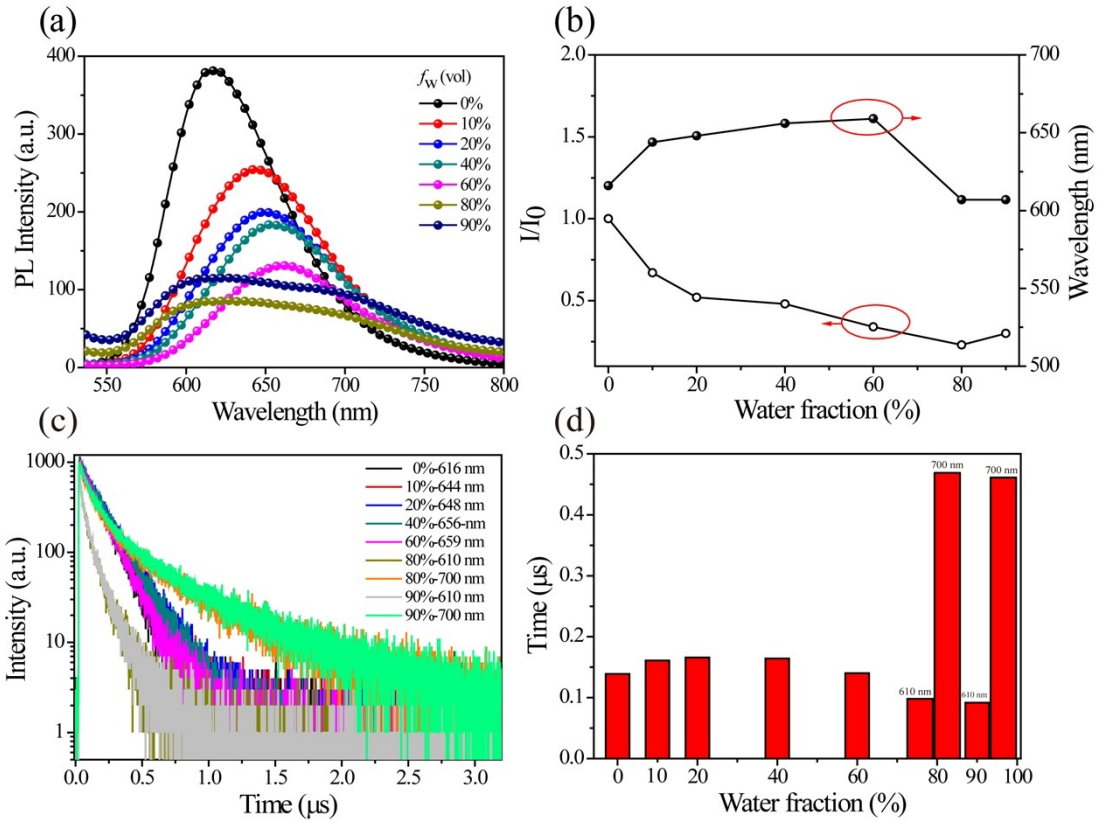

Fig. S10. a) PL spectra of $(DBQ)_2Ir(acac)$ in THF/H_2O mixtures with different water fractions and a concentration of 10^{-5} M at 298 K; b) relationships between the ratio of I/I_0 and the emission maximum *versus* water fraction in THF/H_2O mixtures; I_0 and I were the maximum PL intensity in pure THF and in THF/H_2O mixtures, respectively, Ex=370 nm. c) Transient PL decay spectra of $(DBQ)_2Ir(acac)$ in THF/H_2O mixtures; d) lifetime *versus* water fractions in THF/H_2O mixtures.

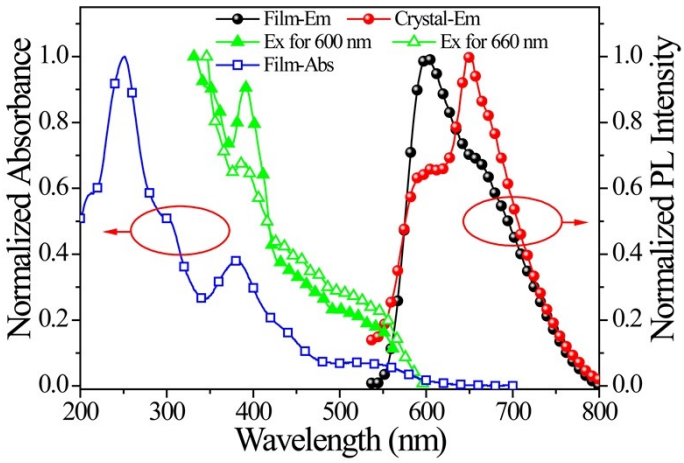

Fig. S11. PL spectra of $(DBQ)_2Ir(acac)$ in film and crystal, Ex=390 nm.

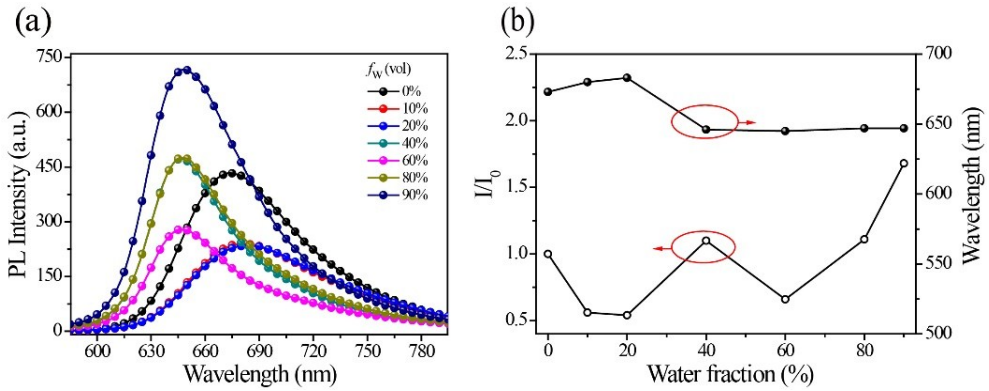

Fig. S12. a) PL spectra of $(DBPz\text{-}11,12\text{-}DO)_2Ir(acac)$ in THF/H_2O mixtures with different water fractions and a concentration of 10^{-5} M at 298 K; b) relationships between the ratio of I/I_0 and the emission maximum *versus* water fraction in THF/H_2O mixtures; I_0 and I were the maximum PL intensity in pure THF and in THF/H_2O mixtures, respectively, Ex=420 nm.

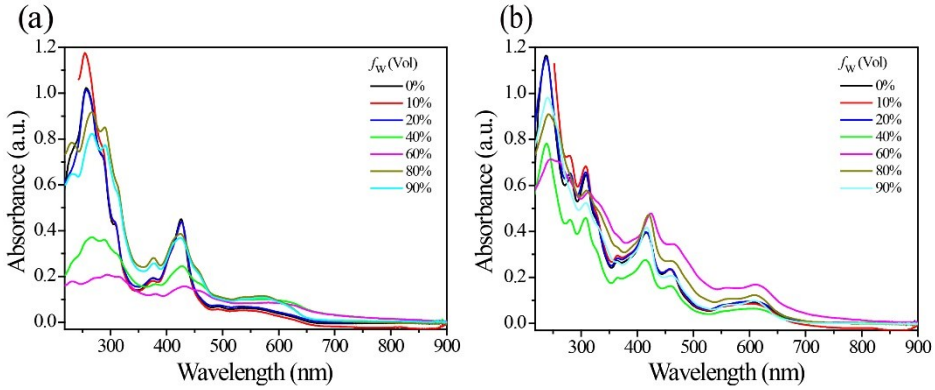

Fig. S13. Absorption spectra of $(DBPz\text{-}11,12\text{-}DO)_2Ir(acac)$ (a) and $(PPz\text{-}11,12\text{-}DO)_2Ir(acac)$ (b) in THF/H_2O mixtures with different water fractions and a concentration of 10^{-5} M at 298 K.

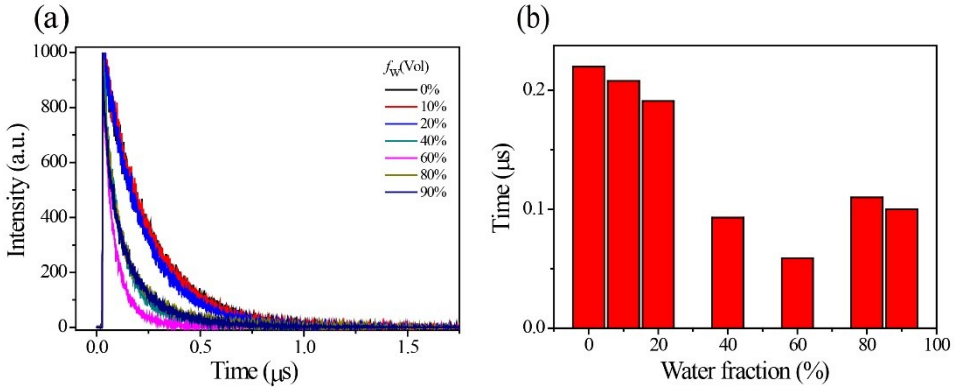

Fig. S14. a) Transient PL decay spectra of $(DBPz\text{-}11,12\text{-}DO)_2Ir(acac)$ in THF/H_2O

mixtures with different water fractions and a concentration of 10^{-5} M at 298 K; b) Column diagrams of decay times *versus* water fractions in THF/H_2O mixtures.

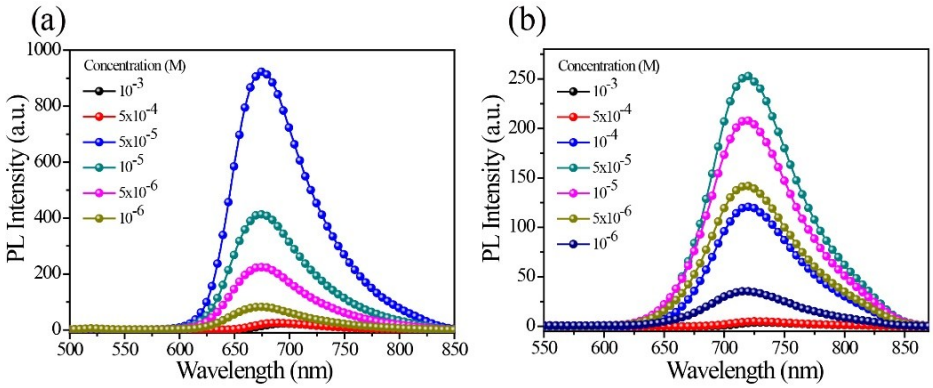

Fig. S15. PL spectra of $(DBPz\text{-}11,12\text{-}DO)_2Ir(acac)$ (a) and $(PPz\text{-}11,12\text{-}DO)_2Ir(acac)$ (b) in THF solution upon concentration from 10^{-3} M to 10^{-6} M, and the absent of the emission spectra of $(DBPz\text{-}11,12\text{-}DO)_2Ir(acac)$ in 10^{-4} M resulted from limitations of the instrument, excited at 420 and 450 nm, respectively.

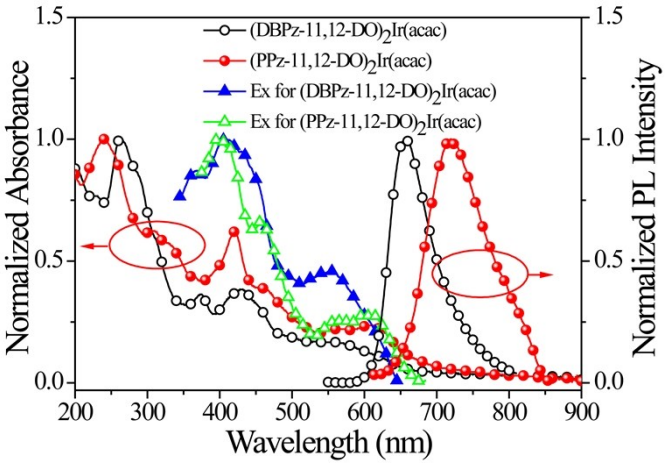

Fig. S16. Absorption, excitation and emission spectra of $(DBPz\text{-}11,12\text{-}DO)_2Ir(acac)$ and $(PPz\text{-}11,12\text{-}DO)_2Ir(acac)$ in neat film, excited at 420 and 450 nm, respectively.

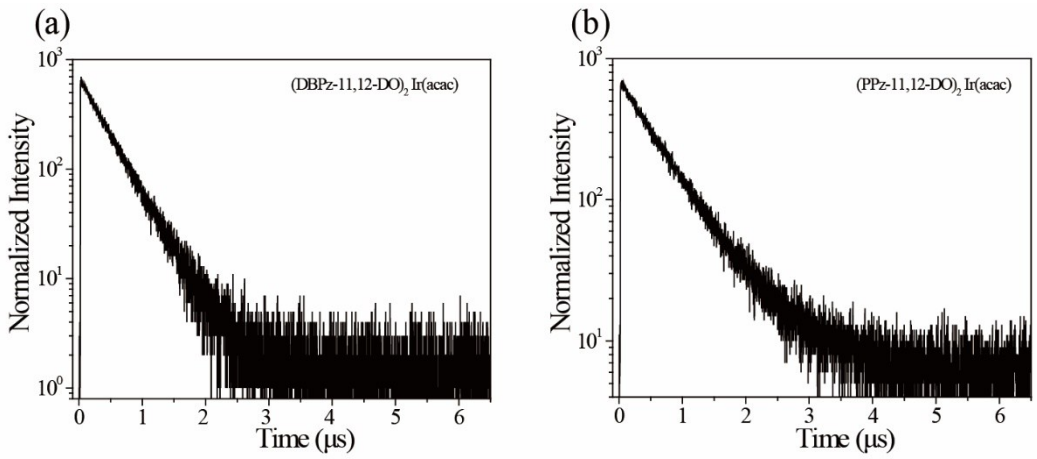

Fig. S17. Transient PL decay curves of $(DBPz\text{-}11,12\text{-}DO)_2Ir(acac)$ (a) and $(PPz\text{-}11,12\text{-}DO)_2Ir(acac)$ (b) in degassed CH_2Cl_2 solutions.

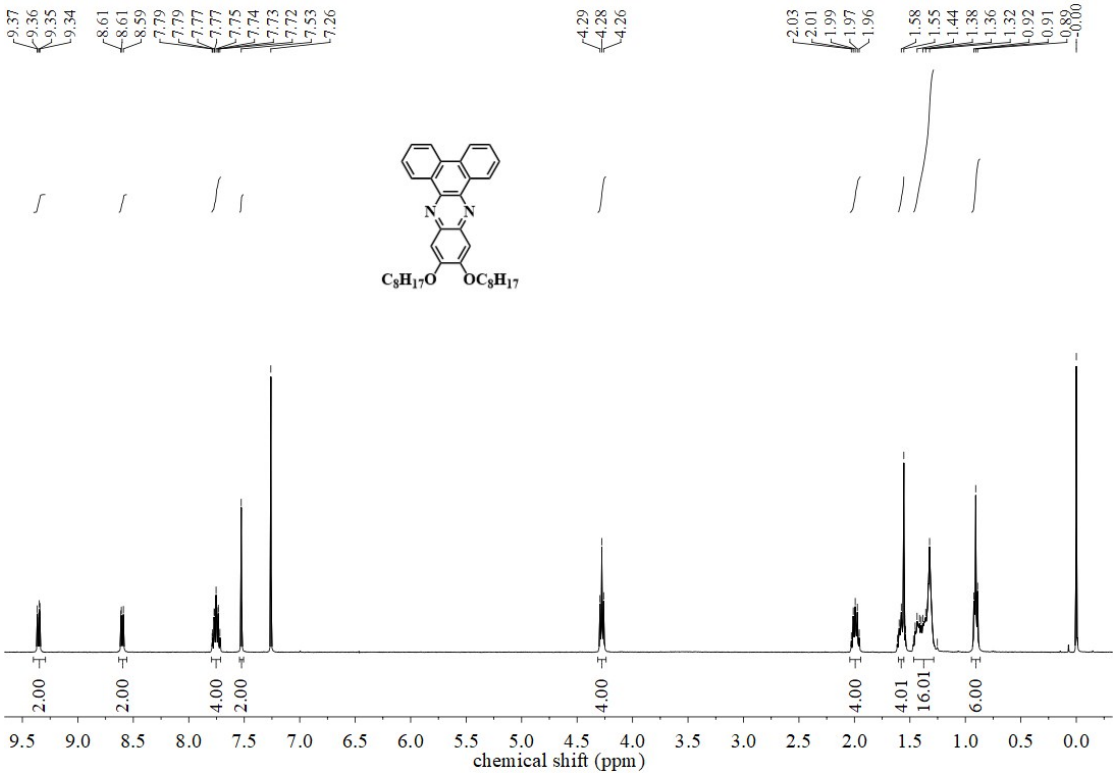

Fig. S18. ^1H NMR spectrum of HDBPz-11,12-DO (400 MHz, $CDCl_3$).

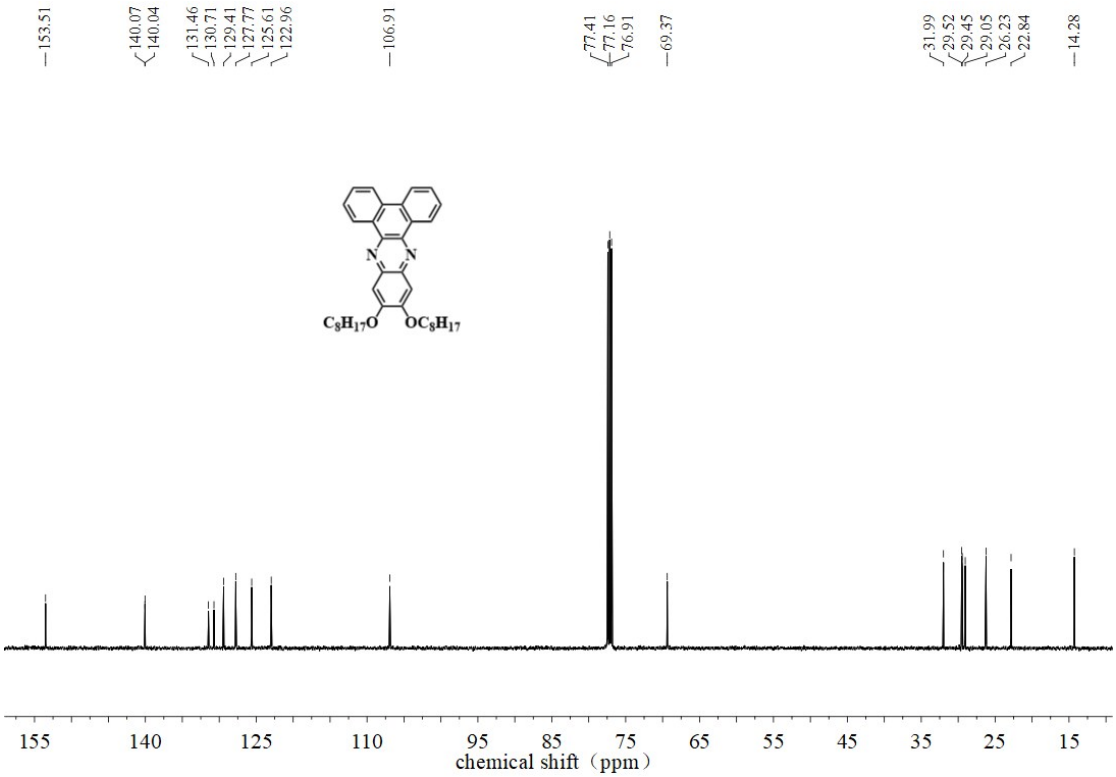

Fig. S19. ^{13}C NMR spectrum of HDBPz-11,12-DO (125 MHz, $CDCl_3$).

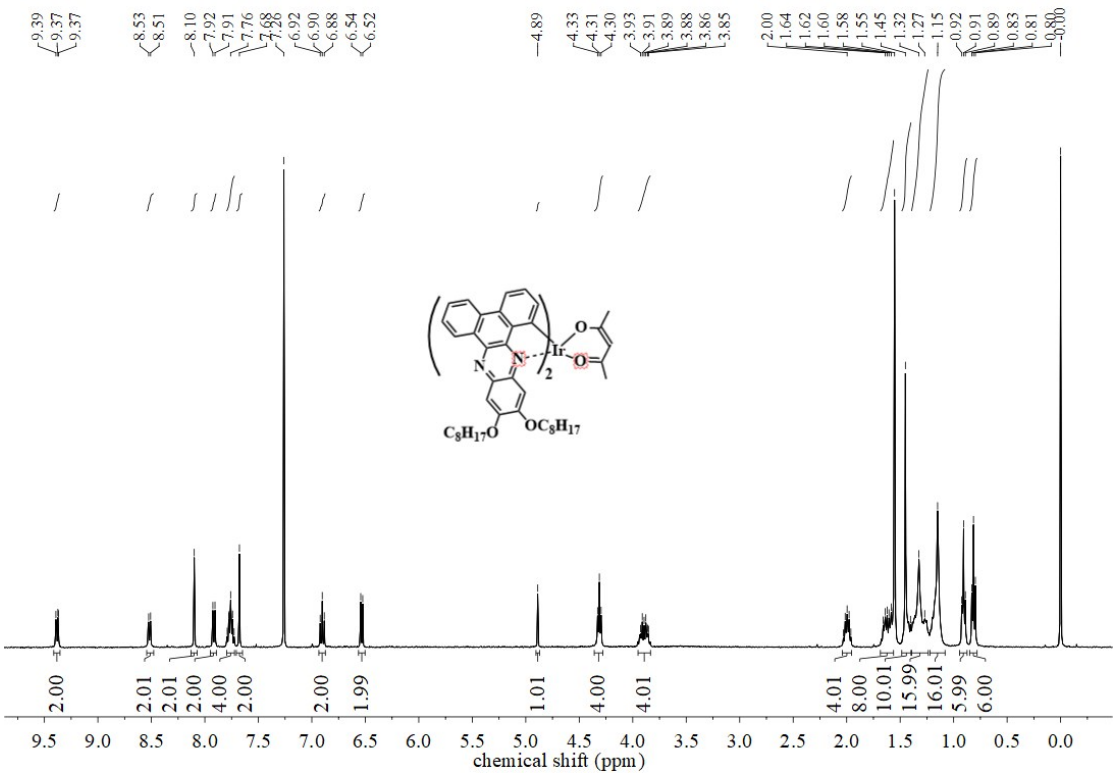

Fig. S20. ^{1}H NMR spectrum of $(DBPz\text{-}11,12\text{-}DO)_2Ir(acac)$ (400 MHz, $CDCl_3$).

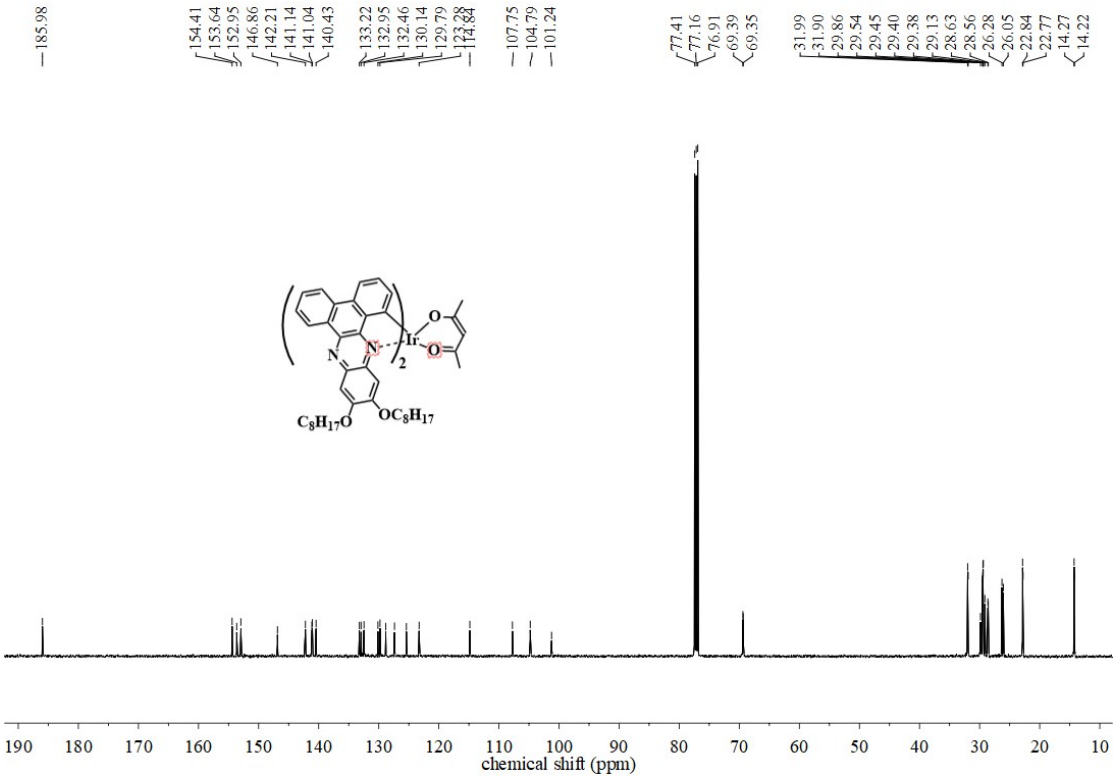

Fig. S21. ^{13}C NMR spectrum of $(DBPz\text{-}11,12\text{-}DO)_2Ir(acac)$ (125 MHz, $CDCl_3$).

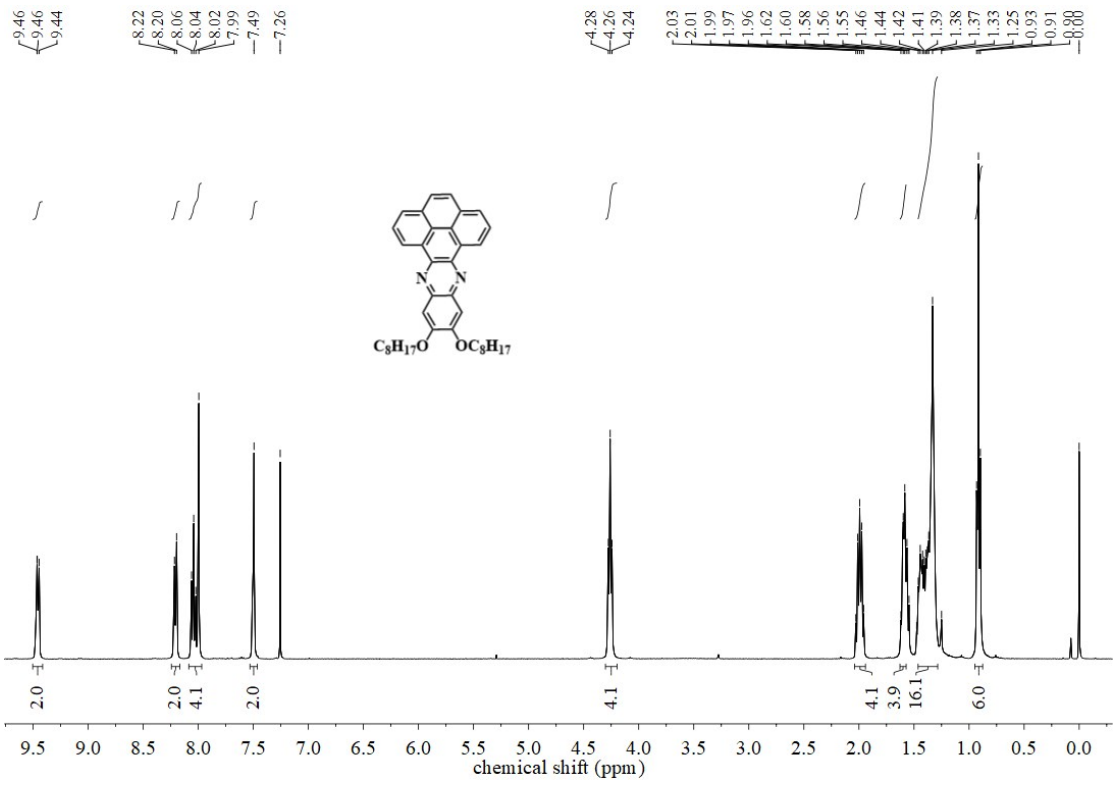

Fig. S22. ^{1}H NMR spectrum of HPPz-11,12-DO (400 MHz, $CDCl_3$).

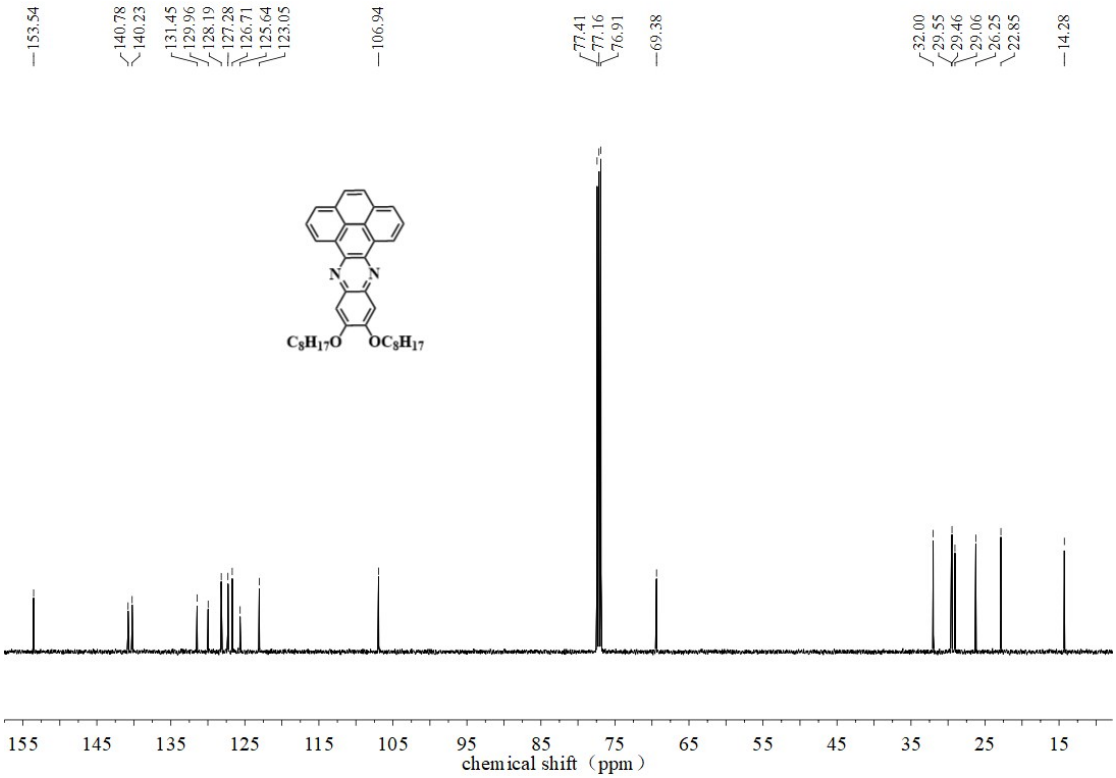

Fig. S23. ^{1}H NMR spectrum of HPPz-11,12-DO (125 MHz, $CDCl_3$).

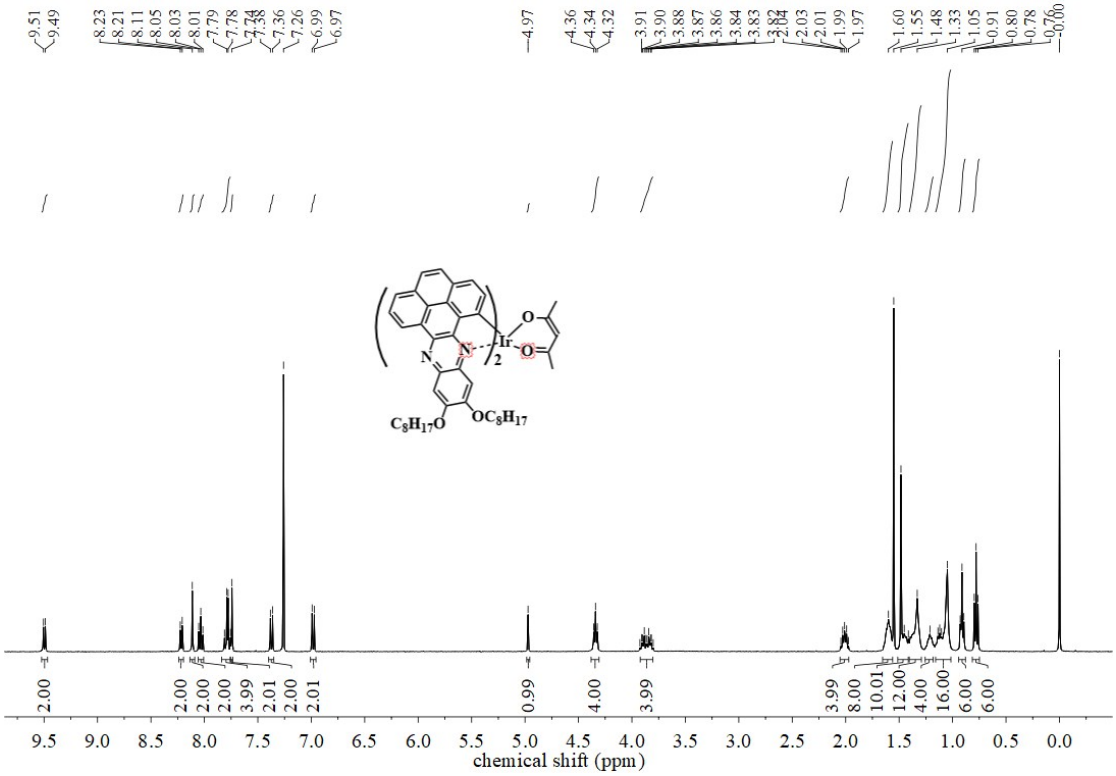

Fig. S24. ^{1}H NMR spectrum of $(PPz\text{-}11,12\text{-}DO)_2Ir(acac)$ (400 MHz, $CDCl_3$).

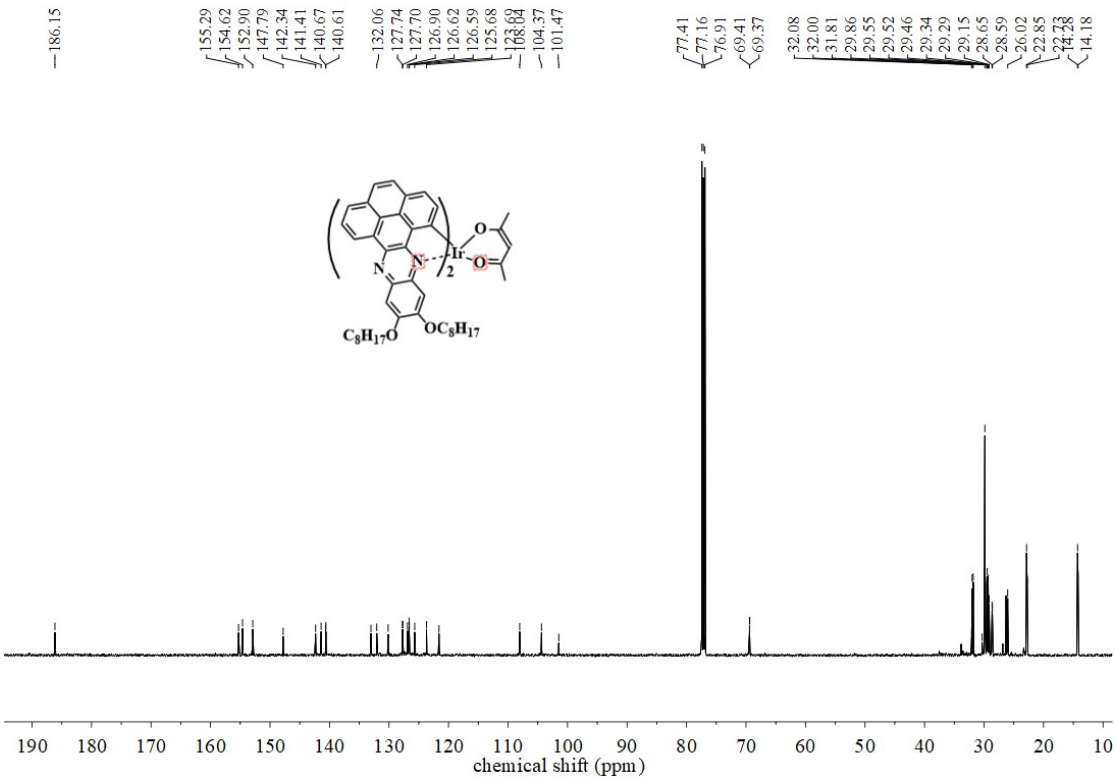

Fig. S25. ^{13}C NMR spectrum of $(PPz\text{-}11,12\text{-}DO)_2Ir(acac)$ (125 MHz, $CDCl_3$).

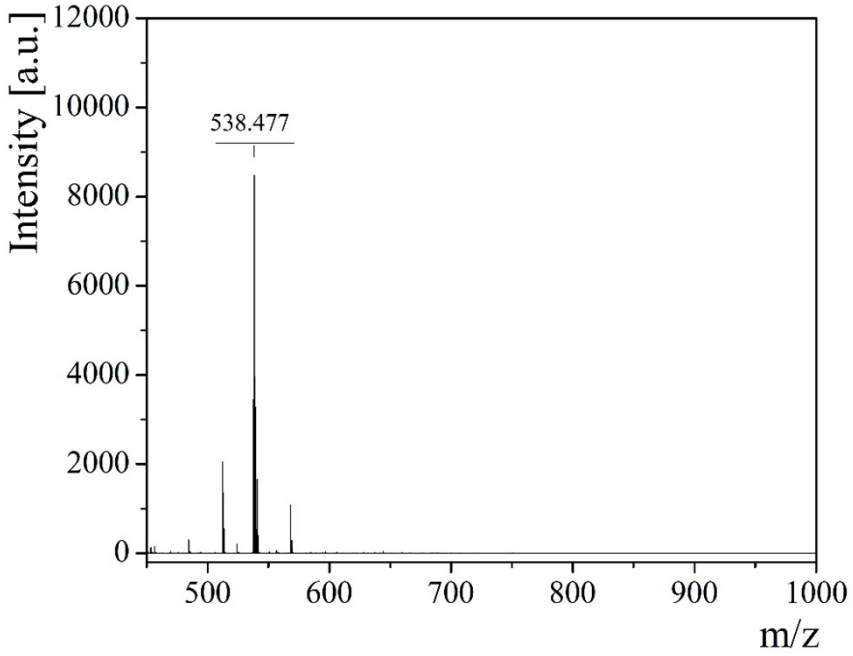

Fig. S26. MALDI-TOF-MS spectrum of HDBPz-11,12-DO.

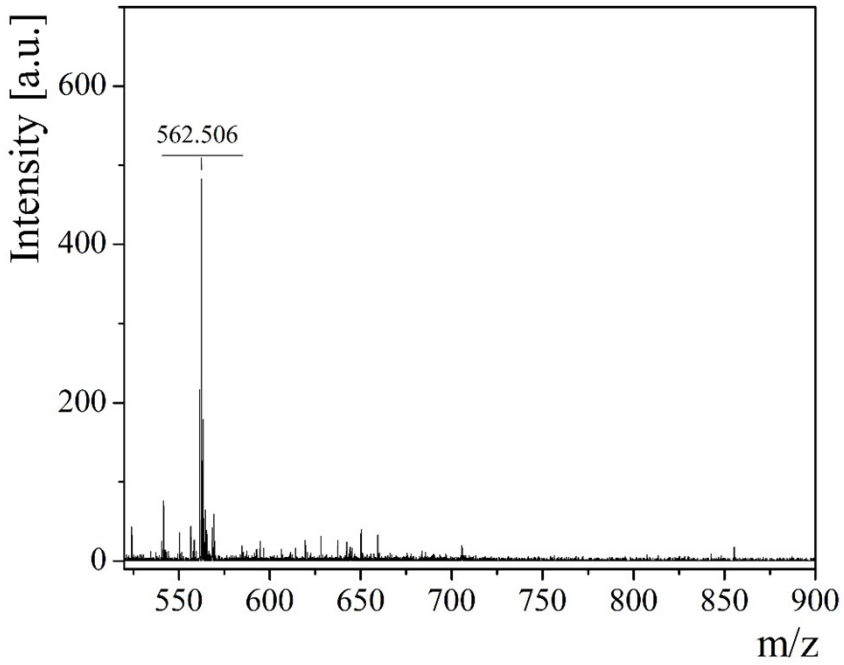

Fig. S27. MALDI-TOF-MS spectrum of HPPz-11,12-DO.

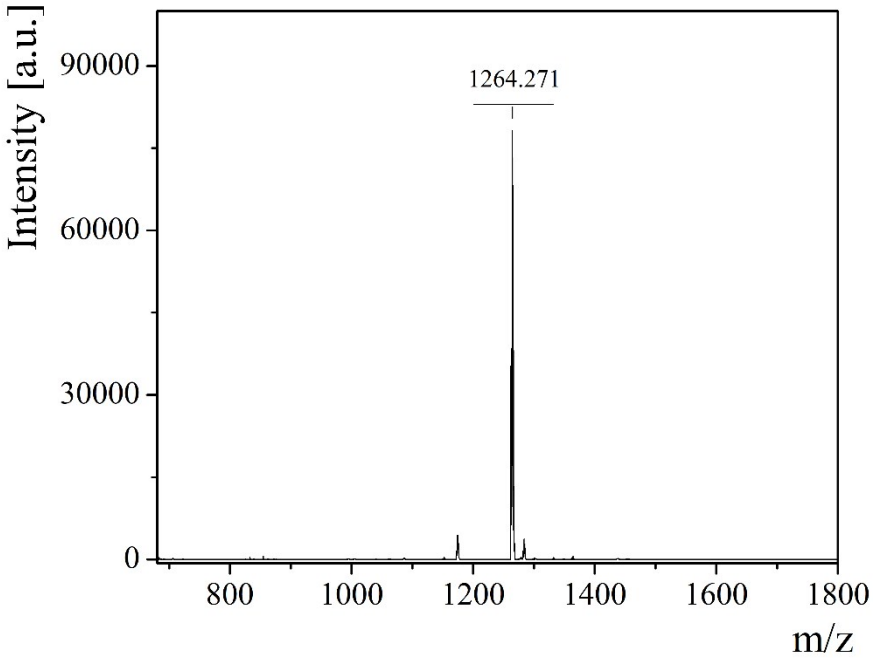

Fig. S28. MALDI-TOF-MS spectrum of $(DBPz\text{-}11,12\text{-}DO)_2Ir(acac)$.

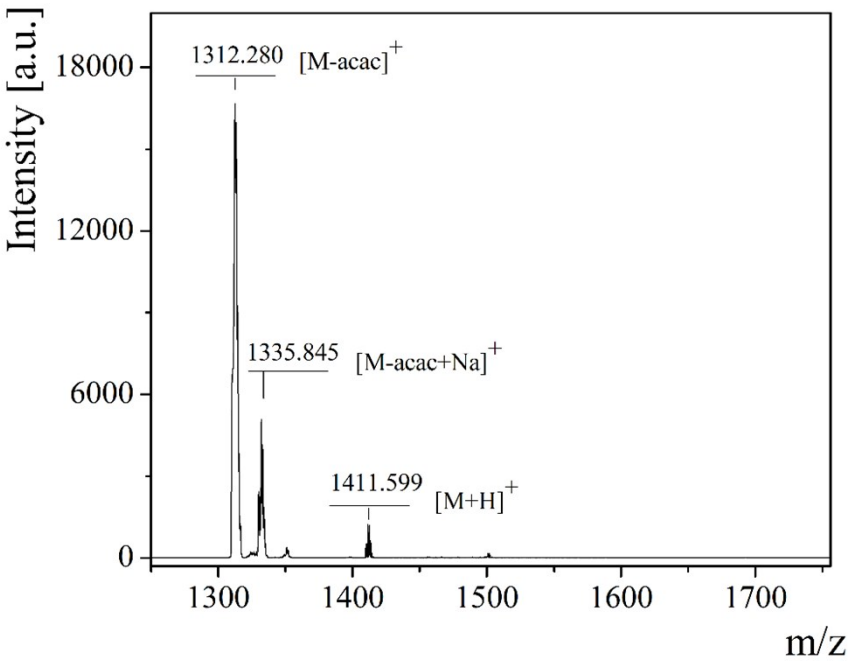

Fig. S29. MALDI-TOF-MS spectrum of $(PPz\text{-}11,12\text{-}DO)_2Ir(acac)$.

Table S1. Crystal data and refinement parameters for complexes $(DBQ)_2Ir(acac)$ and $(PPz\text{-}11,12\text{-}DO)_2Ir(acac)$.

Sample	$(DBQ)_2Ir(acac)$	$(PPz\text{-}11,12\text{-}DO)_2Ir(acac)$
Empirical formula	$C_{38}H_{26}Cl_3IrN_4O_2$	$C_{81}H_{93}IrN_4O_6$
Formula weight	869.18	1410.79
Temperature	173(0) K	296(2) K
Wavelength	0.71073 Å	1.34139 Å
Crystal system	Triclinic	Triclinic
Space group	*P*-1	*P*-1
Unit cell dimensions	a = 9.9655(9) Å b=12.2501(11)Å c = 13.6017(12) Å α = 85.163(2)° β = 88.640(2)° γ = 80.607(2)°	a = 13.2845(7) Å b = 16.5525(8) Å c = 17.2928(11)Å α = 82.589(4)° β = 74.698(4)° γ = 76.485(3)°
Volume	1632.3(3) $Å^3$	3557.0(4)$Å^3$
Z	2	2
Density (calculated)	1.768 mg/m^3	1.317 mg/m^3
Absorption coefficient	4.378 mm^{-1}	2.684 mm^{-1}
F(000)	852.0	1464
Crystal size	0.18 × 0.12 × 0.08 mm^3	0.20 x 0.08 x 0.04 mm^3
Theta range for data collection	3.006 to 55.408°	3.068 to 55.065°
Index ranges	-13<=h<=13, -15<=k<=16, -17<=l<=17	-15<=h<=16, -20<=k<=18, -18<=l<=21

Reflections collected	14843	36841
Independent reflections	7391 [R_{int} = 0.0404]	13393 [R(int) = 0.0660]
Completeness to theta = 53.594°	95.7 %	99.3%
Absorption correction	Semi-empirical from equivalents	
Max/min transmission	0.7508 / 0.4415	0.7508 / 0.4952
Refinement method	Full-matrix-block least-squares on F^2	
Data/restraints/parameters	7391/0/435	13393 / 186 / 834
Goodness-of-fit on F^2	1.030	1.031
Final R indices [I>2sigma(I)]	R_1 = 0.0399, wR_2 = 0.1040	R1 = 0.0623, wR2 = 0.1613
R indices (all data)	R_1 = 0.0478, wR_2 = 0.1088	R1 = 0.0992, wR2 = 0.1898
Extinction coefficient	n/a	n/a
Largest diff. peak and hole	1.66 and -1.37 e. $Å^{-3}$	0.840 and -1.504 e. $Å^{-3}$
CCDC number	1914079	1914075

Table S2. Selected bond lengths (Å) and angles (°) for complex $(DBQ)_2Ir(acac)$

bond lengths (Å)		**Bond angles (°)**	
Ir1-N1	2.036(4)	O2-Ir1-O1	88.18(15)
Ir1-N3	2.034(4)	C17-Ir1-N3	81.51(19)
Ir1-C14	2.014(5)	C14-Ir1-N1	81.75(19)
Ir1-C17	1.990(5)	N3-Ir1-N1	175.22(17)
Ir1-O1	2.146(4)	C14-Ir1-O2	173.00(16)
Ir1-O2	2.145(4)	C17-Ir1-O1	174.03(17)